Scale Design of Dual-Layer Sulfonated Polyphenylsulfone Hol-Low Fiber Membranes for Nanofiltration

Javed Alam *, Arun Kumar Shukla, Lawrence Arockiasamy, Mansour Alhoshan

Posted Date: 20 June 2023

doi: 10.20944/preprints202306.1410.v1

Keywords: Hollow-fiber membranes; dual-layer membranes; nanocomposite membranes; selective separation

Article

Scale Design of Dual-Layer Sulfonated Polyphenylsulfone Hollow Fiber Membranes for Nanofiltration

Javed Alam [1,*], Arun Kumar Shukla [1], Lawrence Arockiasamy [1] and Mansour Alhoshan [1,2]

[1] King Abdullah Institute for Nanotechnology, King Saud University, P.O. Box 2455, Riyadh 11451, Saudi Arabia; javaalam@ksu.edu.sa, ashukla@ksu.edu.sa and ldass@ksu.edu.sa

[2] Department of Chemical Engineering, College of Engineering, King Saud University, P.O. Box 2455, Riyadh 11451, Saudi Arabia; mhoshan@ksu.edu.sa

* Correspondence: javaalam@ksu.edu.sa

Abstract: The study presents the synthesis and characterization of dual-layer sulfonated polyphenylenesulfone (SPPSu) nanocomposite hollow fiber nanofiltration membranes incorporating titanium dioxide (TiO_2) nanoparticles using the phase inversion technique. The newly developed membranes were systematically characterized using advanced tools and methods to evaluate their properties and performance. The study focused on investigating the effects of TiO_2 addition in the SPPSu inner layer on pure water permeability, and salt rejection. The nanocomposite hollow fiber nanofiltration membranes exhibited a significant enhancement in pure water permeability, with a three-fold increase compared to the pristine membranes, achieving a flux of 5.4 L/m^{2}h.bar. The addition of TiO^2 also led to an improvement in the mechanical properties of the membranes, as evidenced by the increase in the expected tensile strength from 2.4 to 3.9 MPa. To evaluate the salt rejection performance, rejection tests were conducted using a laboratory-scale filtration setup in recycle mode. Aqueous solutions containing different divalent ions, specifically magnesium sulfate (Mg_2SO_4) and sodium sulfate (Na_2SO_4) at a concentration of 500 ppm, were used as the feed solution. The modified dual-layer hollow fiber nanocomposite membranes exhibited a maximal rejection of 95% for Mg_2SO_4, demonstrating their effective separation capabilities for divalent ions. The findings of this study highlight the successful synthesis and characterization of dual-layer SPPSu nanocomposite hollow fiber nanofiltration membranes incorporating TiO_2 nanoparticles. The incorporation of TiO_2 resulted in improved pure water flux, mechanical strength, and salt rejection performance. These enhanced properties make the developed nanocomposite membranes promising candidates for applications in nanofiltration processes, particularly for the selective separation of divalent ions from aqueous solutions.

Keywords: Hollow-fiber membranes; dual-layer membranes; nanocomposite membranes; selective separation

1. Introduction

Water scarcity has become a critical global issue impacting numerous regions worldwide. Factors such as population growth, urbanization, and climate change have exacerbated the demand for clean and fresh water, while the availability of freshwater resources continues to diminish. This escalating water scarcity necessitates innovative solutions to address the challenge and ensure sustainable water management practices [1–4].

Membrane technology has emerged as a crucial tool in tackling water scarcity by offering efficient and effective water treatment and purification solutions. Membrane-based processes provide several advantages, including high efficiency, low energy consumption, and the ability to remove contaminants at the molecular level [3]. These processes find extensive application in desalination, wastewater treatment, and water reuse. Among various membrane configurations, hollow-fiber membranes have gained significant attention in academia and industry due to their inherent advantages, including a large surface area per unit volume, favorable mechanical strength, and ease of handling. However, the performance of conventional hollow-fiber membranes requires

 doi:10.20944/preprints202306.1410.v1

further improvement to achieve highly selective separation while maintaining enhanced thermal and mechanical stability [5–12].

In response to these challenges, researchers have directed their focus towards the development of dual-layer hollow-fiber (DLHF) membranes, which offer the potential for a selective surface layer with a mixed matrix. This unique characteristic enables highly selective separation while maintaining excellent mechanical strength, allowing for long-term operation without fiber failure or significant deterioration. Recent studies have demonstrated successful applications of DLHF membranes in various separation processes [13–15]. The fabrication of dual-layer hollow fiber membranes has garnered considerable interest due to its numerous advantages, including low material cost, favorable thermal and mechanical stability, and the ability to optimize membrane performance using high-performance selective layers [12,16–18]. Notable advancements in this field include the work of Liu et al. [15], who reported the fabrication of a dual-layer hollow-fiber membrane using poly(styrene-b-4-vinylpyridine)-based (PS4VP-based) and poly(vinylidene fluoride)-based (PVDF-based) materials. The membrane was fabricated using block copolymer self-assembly through non-solvent induced phase separation, resulting in a highly ordered isoporous surface and excellent mechanical strength. Furthermore, dual-layer nanocomposite hollow fiber membranes composed of polyethersulfone (PES) and PVDF, incorporating multi-walled carbon nanotubes (MWCNTs), have been successfully fabricated using a two-step thermally induced phase separation/non-solvent induced phase separation (TIPS/NIPS) process. These membranes exhibited the ability to withstand high pressures with relatively low membrane compaction, making them suitable for ultrafiltration applications. The fabrication of novel dual-layer hollow-fiber membranes using a single-step co-extrusion technique has also been explored by Dzinun et al.[19]. These membranes incorporated immobilized titanium dioxide (TiO_2) nanoparticles in their outer layer, exhibiting favorable interfacial adhesion and well-dispersed TiO_2 particles. Comparative studies revealed the superior mechanical strength of DLHF membranes compared to flat sheet cellulose acetate (CA) membranes, with smaller pore sizes in the outer layer of the hollow-fiber membranes. Additionally, dual-layer hollow-fiber membranes based on polybenzimidazole (PBI) and PES materials have demonstrated high rejection rates for heavy metals such as cadmium, lead, and chromium, as reported by Zhu et al.[14]. These advancements highlight the progress made in the field of dual-layer hollow fiber membranes, showcasing the potential for enhanced membrane performance and the utilization of various functional materials to achieve specific separation requirements.

Polyphenylsulfone (PPSu) stands out as an especially promising membrane material for ultrafiltration, nanofiltration, reverse osmosis, and forward osmosis. PPSu possesses desirable characteristics, including ease of membrane formation and favorable thermal and mechanical stability, making it an ideal choice for membrane materials [20]. Moreover, PPSu exhibits superior properties compared to commonly used materials like polysulfone (PSf) and polyether sulfone (PES). Furthermore, the relatively low cost of PPSu resin enhances its appeal as an alternative for next-generation membrane preparation. However, similar to PSf and PES, PPSu is prone to fouling due to its hydrophobic nature. Fouling not only increases the frequency of membrane cleaning and energy expenditure required to maintain productivity but also necessitates larger membrane areas and frequent membrane replacements. Therefore, alternative approaches must be explored to develop more hydrophilic membranes through chemical modification, surface membrane functionalization, and incorporation of nanoparticles within the membrane matrix (MMM) [21–24]. The incorporation of different nanomaterials in polymer matrices has gained significant attention due to their ability to impart unique properties to the resulting polymer nanocomposites. Various types of nanomaterials have been explored for their incorporation, including carbon-based nanomaterials such as carbon nanotubes (CNTs) and graphene, metallic nanoparticles such as silver (Ag) and gold (Au), metal oxide nanoparticles such as titanium dioxide (TiO_2) and zinc oxide (ZnO), and clay nanoparticles like montmorillonite (MMT) and halloysite nanotubes (HNTs). Each of these nanomaterials offers distinct characteristics that can be beneficially transferred to the polymer matrix [25–31].

The main objective of this work is to design and fabricate dual-layer sulfonated polyphenylsulfone nanocomposite hollow fiber nanofiltration membranes for high-efficiency salt

 doi:10.20944/preprints202306.1410.v1

separation. By incorporating innovative strategies such as chemical modification, surface membrane functionalization, and nanoparticle loading within the inner surface of membrane matrix, these membranes aim to enhance their hydrophilicity, surface charge, surface morphology, and achieve high-efficiency salt separation.

2. Materials and Methods

2.1.Materials

Polyphenylsulfone (PPSu) was kindly supplied by Solvay Advanced Polymers, Italy, and served as the main polymer matrix for the fabrication of the membranes. Polyethylene glycol-600, magnesium sulfate, sodium sulfate, sodium hydroxide, potassium chloride, sodium azide, and glycerol were obtained from Merck and used as received. Chlorosulfonic acid, an important reagent in the synthesis of sulfonated polyphenylenesulfone (SPPSu), was also obtained from Merck. Titanium dioxide nanoparticles, which played a crucial role in enhancing the properties of the membranes, were obtained from Sigma Aldrich. Sodium dodecyl sulfate (SDS), a surfactant, was also obtained from Sigma Aldrich and used in the membrane preparation process. N, N-Methyl Pyrrolidone and dichloromethane were sourced from SD Fine-Chem Limited, India, and used as solvents in the synthesis and processing of the membranes. Millipore MQ purified water was used for the experiments and to prepare the gelation bath, ensuring the purity of the water used in the membrane fabrication process.

2.2. Synthesis of Sulfonated Polyphenylsulfone

The synthesis of sulfonated polyphenylsulfone (SPPSu) was conducted using a procedure reported in the literature, involving the use of chlorosulfonic acid. Initially, predried PPSu was dissolved in dichloromethane (DCM) by constant stirring. The chloro sulfonic acid was slowly added to the DCM solution over a period of 2 hours at 0 °C using a dropping funnel. The resulting solution, which became viscous, was further stirred for 2 hours at room temperature. To precipitate the SPPSu, the viscous polymer solution was treated with ethanol, and the resulting precipitate was thoroughly washed until the pH reached 7. The obtained white precipitate of SPPSu was then dried for 24 hours in a vacuum oven. To modify the SPPSu, it was re-dissolved in NMP, and an excess amount of sodium methoxide was added. The mixture was continuously stirred for 3 hours to allow for the reaction to take place. The sodium salt of SPPSu was then re-precipitated in distilled water and subsequently dried in a vacuum oven. The resulting dried SPPSu exhibited a highly crystalline structure, making it suitable for the preparation of hollow-fiber membranes and blend nanocomposite hollow-fiber membranes. This synthesis procedure provided a reliable method for obtaining sulfonated polyphenylenesulfone with desired properties. The highly crystalline nature of the SPPSu ensured its stability and enhanced performance in subsequent membrane fabrication processes. The sodium salt modification introduced additional functional groups into the polymer matrix, expanding its potential applications and allowing for further customization of the resulting membranes. Overall, this synthesis process laid the foundation for the preparation of hollow-fiber membranes and blend nanocomposite hollow-fiber membranes with improved properties and performance.

2.3. Fabrication of DLHF nanocomposite membrane and module

The fabrication process of the dual-layer hollow-fiber nanocomposite membrane and module is described in detail as follows.

First, PPSu, SPPSu, and TiO_2 nanopowder were dried overnight at 60 °C in a vacuum oven to eliminate moisture content. The concentrations of the dope solutions were determined based on the viscosity-concentration profile. A 24 wt% PPSu solution was chosen as the outer dope solution, while a 22 wt% SPPSu solution was used as the inner dope solution. For the inner dope solution, TiO_2 was dispersed in NMP and sonicated for 40 minutes using a Branson digital probe sonicator. After sonication, the TiO_2 dispersion was mixed with the SPPSu polymer solution. The outer dope solution was prepared by directly adding PPSu polymer into NMP solvent. The specific blend compositions

Preprints (www.preprints.org) | NOT PEER-REVIEWED | Posted: 20 June 2023 doi:10.20944/preprints202306.1410.v1

are provided in Table 1. Both mixtures were stirred at 70 °C for 24 hours to achieve a homogeneous solution and subsequently degassed in a sealed container for 12 hours to remove any trapped air bubbles.

Table 1. Dual-layer hollow-fiber membrane blend composition

Membranes	Inner layer			Outer layer		
	SPPSu (wt%)	TiO_2 (wt%)	NMP (wt%)	PPSu (wt%)	PEG 600 (wt %)	NMP (wt%)
SPPSu/PPSu	22	--	78.0	24	2.0	74
SPPSu-TiO_2 (0.50 wt%)/PPSu	22	0.50	77.5	24	2.0	74
SPPSu-TiO_2 (1.0 wt%)/PPSu	22	1.0	77.0	24	2.0	74
SPPSu-TiO_2 (2.0 wt%)/PPSu	22	2.0	76.0	24	2.0	74

During the spinning process, a bore fluid composed of a 9:1 ratio of double distilled water and NMP was used. Tap water served as the external coagulant. Hollow-fiber membranes were prepared using a hollow fiber spinning line from DELTAE, Italy. The spinning process involved employing triple-orifice spinnerets and a spinning machine, as shown in Figure 1 and spinning conditions of dual-layer hollow-fiber membranes provided in Table 2. The spun hollow-fiber membranes were then immersed in a water bath for 24 hours to remove residual solvent. To improve membrane wettability and prevent pore collapse, the membranes underwent post-treatment using a 20% glycerol solution for 1 hour. Following post-treatment, the membranes were dried at room temperature for 72 hours before module fabrication.

Table 2. Spinning conditions of dual-layer hollow-fiber membranes

Parameter	Value
Bore fluid composition (wt%)	Water/NMP(9:1)
External coagulant	Water
Outer dope flow rate (ml/min)	4
Inner dope flow rate (ml/min)	8
Bore fluid flow rate (ml/min)	2
Air gap (cm)	10
Take up speed (m/min)	2
Spinneret temperature (° C)	50

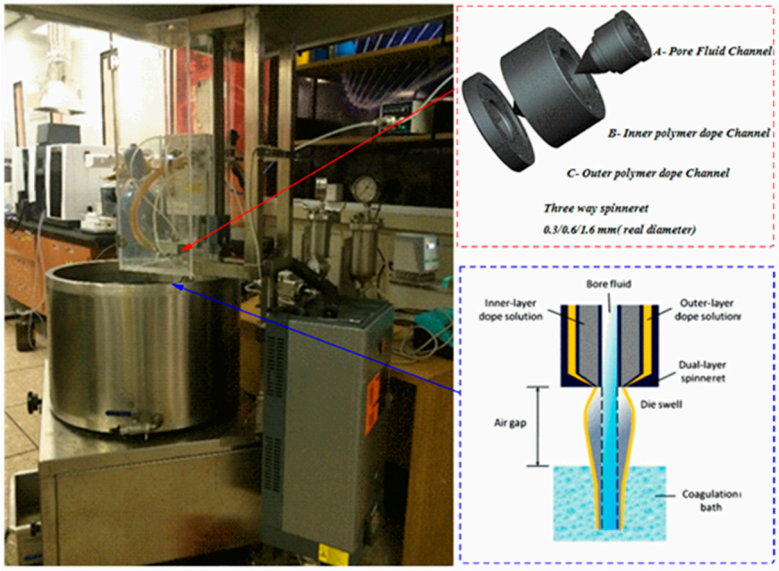

Figure 1 Schematic representation of dual-layer hollow-fiber membrane

Preprints (www.preprints.org) | NOT PEER-REVIEWED | Posted: 20 June 2023 doi:10.20944/preprints202306.1410.v1

For module preparation, defect-free hollow fibers (100 in total) were selected. These hollow fibers were wrapped with a polymeric mesh and inserted into acrylic-based modules. The ends of the module were sealed using epoxy resin. Freshly prepared epoxy resin was poured onto the module through the permeate pathway. The module was shaken thoroughly and then dried. A representation of the prepared module can be seen in Figure 2.

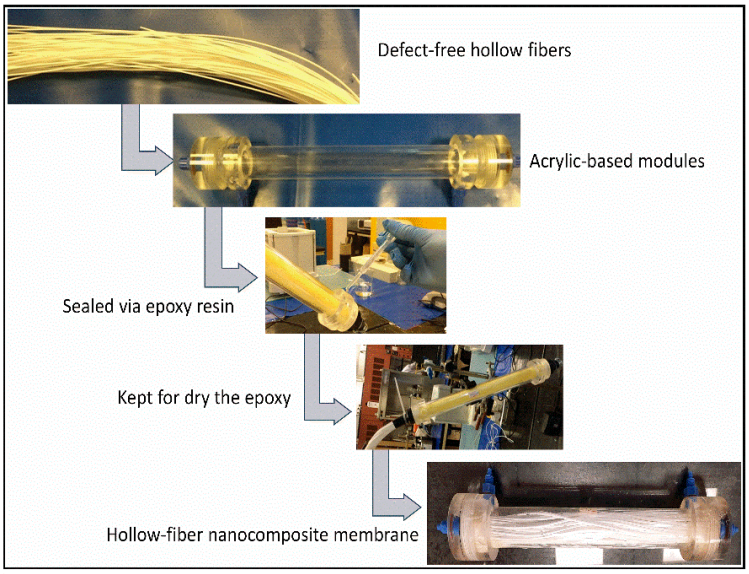

Figure 2. A representation of the preparation of module

2.4. Rheological properties of dope solution

The rheological properties of the dope solution were evaluated using an MCR300 rheometer from Anton Parr (Austria). The measurements were conducted with a PP50 measuring plate having a diameter of 50 mm and a measuring position gap of 1 mm. The angular frequency (ω) of the rheometer was set in the range of 0.01 to 100 rad/s to obtain the necessary rheological parameters and viscosity values. All experiments were conducted under a nitrogen atmosphere to prevent any unwanted reactions or interactions.

2.5. Membrane characterization

2.5.1. Morphological studies

The cross-sectional morphology of the prepared DLHF membrane was analyzed using Scanning Electron Microscopy (SEM) with a JEOL instrument from Japan. Prior to imaging, the membrane samples were allowed to air dry to remove any surface water. The dried samples were then fractured under cryogenic conditions using liquid nitrogen and further dried at a temperature of 21 °C. To enhance the electrical conductivity of the polymeric membranes for SEM imaging, a thin layer of gold was sputtered onto the sample surface. The SEM images were captured under a high vacuum environment at an operating voltage of 5–15 kV, depending on the specific characteristics of the sample being analyzed. This allowed for detailed visualization and examination of the cross-sectional structure of the dual-layer nanocomposite hollow fibers. The SEM images provided insights into the internal morphology, layer arrangement, and overall integrity of the membranes.

Furthermore, Atomic Force Microscopy (AFM) was employed to characterize the surface features of the membranes, such as texture and roughness. Surface imaging was conducted in tapping mode at ambient temperature using a silicon (Si) tip. The AFM measurements were performed with a scan frequency of 0.999 Hz using the Veeco NanoScope V MultiMode software. The scan ranges for surface roughness and structure analysis were set at 5 × 5 μm and 500 × 500 nm, respectively. By utilizing AFM, the topography and surface properties of the DLHF could be examined at a nanoscale

Preprints (www.preprints.org) | NOT PEER-REVIEWED | Posted: 20 June 2023 doi:10.20944/preprints202306.1410.v1

level, providing information about the surface roughness, texture, and any potential surface modifications or enhancements.

2.5.2. Measurement of membrane zeta potential

The zeta potential of a manufactured hollow fiber (HF) membrane (inner surface) was measured using the tangential streaming potential method using a SurPASS" electrokinetic analyzer (Anton Paar, GmbH, Austria). The membrane sample was preserved to a length of 5mm and put into a sample holder of HF membrane with a diameter of 1.4 mm. The zeta potential of the inner surface of a hollow fiber membrane as a function of pH was calculated using a 1mM KCl electrolyte solution. SurPASS's in-built titration device has been used to test the streaming potential under various pH conditions ranging from pH 6 to pH 2 and pH. In addition, the pH of the electrolyte solution was adjusted using a titration device and 0.05 M HCl and 0.05 M NaOH. Finally, Attract® software estimated Zeta potential from streaming potential readings using the Fairbrother and Mastin (F-M) equation provided in Equation 1:

$$\zeta = \frac{\Delta U}{\Delta p} \times \frac{\eta}{\varepsilon \times \varepsilon_0} \times \frac{L}{D} \quad (1)$$

Where, ΔU and ΔP are streaming potential (mV), applied pressure (Pa); and L & D are the channel length (m) as well cross section area (m^2), respectively.

2.5.3. Porosity and Contact Angle Measurement

The porosity of the hollow fibers is determined by soaking the membranes in kerosene for 2 days. The residual kerosene on the surface of the hollow fibers will be removed by blotting with tissue paper. The mass of the membranes before and after immersing in kerosene will be obtained using a digital microbalance. The porosity of the membranes (ε) is defined as the pore volume divided by the total volume of the membrane as follows:

$$\varepsilon(\%) = \frac{(W_w - W_d)}{(W_w - W_d)/(\rho_w - \rho_p)} \times 100 \quad (2)$$

Where, Ww is the mass of the kerosene-soaked membrane (g), Wd is the mass of the dry membrane (g), ϱw is the kerosene density (0.82 g/cm^3) and ϱp is the density of the polymer.

The contact angle of the hollow-fiber membranes was measured by the sessile drop technique. Ten different locations had their contact angles measured, and the average results were then given. The drop-shape analysis system was entirely automated, and the contact angles were measured.

2.5.4. Thermal and Mechanical properties of the membranes

A Thermogravimetric analyzer (METTLER) was used to monitor the degradation temperature while heating the manufactured hollow-fiber membranes at a rate of 10 ° C min-1 in order to examine their thermal stability.

The Double column Lloyd (UTM 5KN Model LR5K Plus) was used to test the mechanical parameters of the hollow fibres at room temperature, including extension at break, tensile strain, and the Young's modulus. In order to get reliable findings, at least five membrane samples per membrane were analysed.

2.5.5. Performances of the membranes

The permeability of pure water through the membranes will be determined by measuring the time required for the permeation of a specific amount of water. The flux of water will be calculated using the following formula:

$$J_w = \frac{V}{A\,t} = \frac{Q}{A\,\Delta t} \quad (3)$$

Preprints (www.preprints.org) | NOT PEER-REVIEWED | Posted: 20 June 2023 doi:10.20944/preprints202306.1410.v1

where, J_w is the water flux (L/m² h); Q is the quantity of water permeated (l); Δt is the sampling time (h); and A is the membrane area (m²).

The rejection performances of the membrane module were evaluated using a cross-flow system operating in total recycle mode. Two distinct salt solutions, Na_2SO_4 and MgSO4, were prepared with an identical concentration of 500 ppm. The experiments were conducted at a pressure of 3 bar and neutral pH conditions. Solute rejection was determined by calculating the ratio between the permeate concentration (Cp) and the feed concentration (Cf) using equation 6. The concentrations of the feed and permeate samples were analyzed using Ion Chromatography (ICS 5000-DIONEX) to determine the rejection ability of the membrane module.

$$Rejection\ \% = 1 - \frac{Cp}{Cf} \times 100 \quad (4)$$

All experiments were conducted three times to minimize errors, and the average values were calculated.

3. Results and Discussion

3.1. Rheological properties of the dope solution

The high viscosity of the solution indicates that the overall diffusion between components in the phase-inversion system is hindered kinetically. This can be attributed to an increase in rheological hindrance or a delayed exchange between the solvent and non-solvent, which ultimately affects the characteristics of the resulting membranes. Therefore, conducting rheological studies on the dope solution is crucial for enhancing membrane performance. In order to determine the inner and outer dope solution viscosity at the hollow-fiber spinning temperature of 50 °C, the viscosity was measured as a function of shear rate. The results of this study are presented in Figure 3. It was observed that the viscosity of the SPPSu-TiO_2 (1.0 wt%) dope solution exhibited a significant increase compared to that of the SPPSu solutions. This can be attributed to the addition of TiO_2 nanoparticles in the solution. Overall, these findings emphasize the importance of understanding and controlling the rheological properties of the dope solution, as it directly impacts the performance of the resulting membranes.

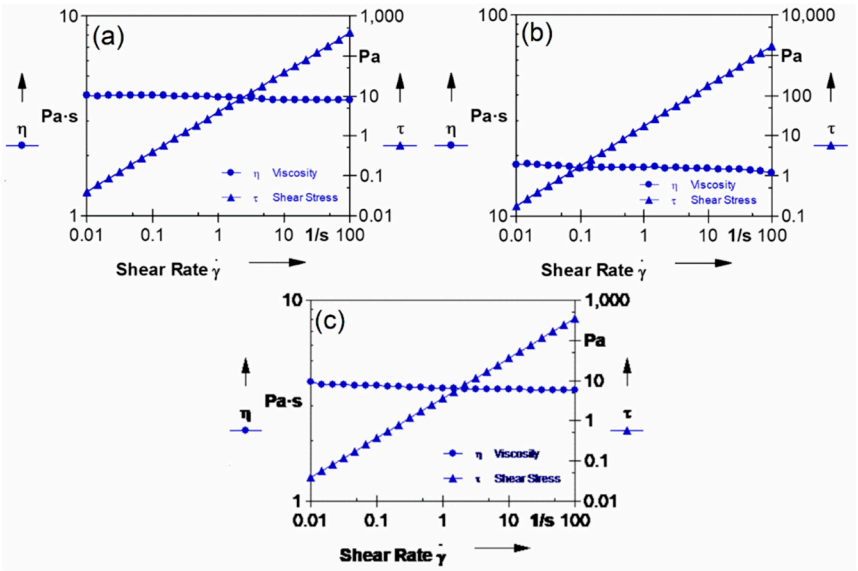

Figure 3. Rheological properties of the (a) PPSu (b) SPPSu and (c) SPPSu-TiO_2 (1.0wt%) dope solution.

3.2. Membrane morphology

Preprints (www.preprints.org) | NOT PEER-REVIEWED | Posted: 20 June 2023 doi:10.20944/preprints202306.1410.v1

In this study, Figure 4a–d presents the SEM images illustrating the cross section of the DLHF membranes that were prepared. It is noteworthy that delamination between the two layers was observed, which can be attributed to the fact that the inner and outer dope solutions were synthesized using the same material. Despite the delamination, the cross section morphology of the hollow fibers exhibited a moderately symmetric structure in both the inner and outer layers of the membrane. The morphology of the hollow fibers is influenced by the concentrations of polymer dope and the air gap employed in the fabrication process. In this investigation, a constant air gap of 10 cm was maintained, indicating that the primary factor impacting the morphology is the polymer concentration in the starting dope solution. Detailed information regarding the specific concentrations used can be found in Table 1 of the manuscript. Regarding the addition of different concentrations of TiO_2 into the SPPSu polymer matrix in the inner layer, the images clearly demonstrate that this addition resulted in significant structural changes in the cross section of the membranes. The morphology of the DLHF nanocomposite membrane reveals a very thin top layer with nanopores. On the other hand, the incorporation of PEG 600 on the outer surface of PPSu accelerated the demixing of the solvent and non-solvent, leading to the formation of microvoids in the cross section of the outer layer. Importantly, the cross-section SEM morphology images of the produced membranes were found to be in agreement with the water permeability results obtained, indicating a correlation between the observed structural features and the transport properties of the membranes.

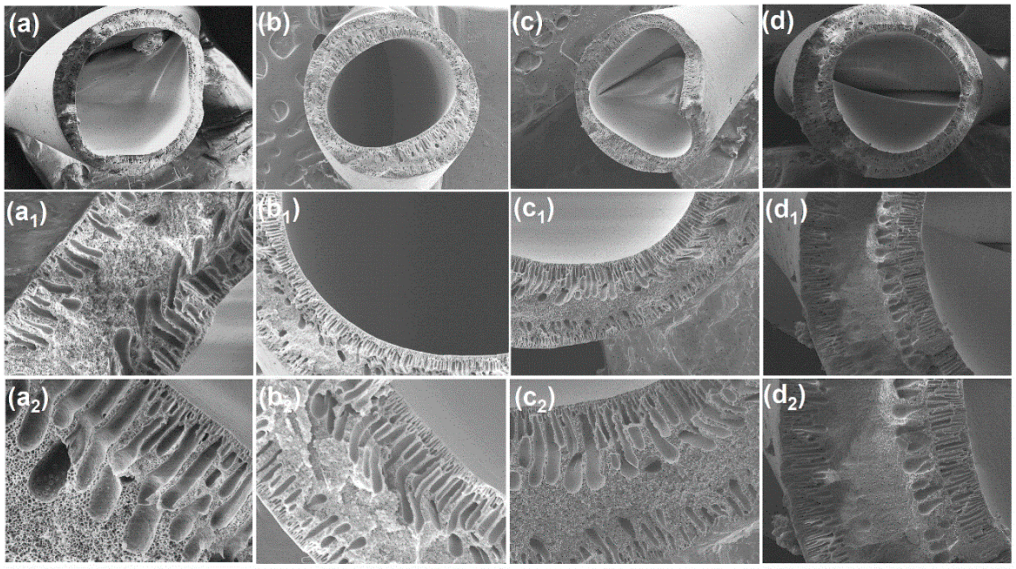

Figure 4. SEM cross-sectional images with high magnifications of (a) SPPSu/PPSu, (b) SPPSu-TiO_2 (0.50 wt%)/PPSu, (c) SPPSu-TiO_2 (1.0 wt%)/PPSu, and (d) SPPSu-TiO_2 (2.0 wt%)/PPSu membranes.

Moreover, the inner layer surface roughness of the prepared DLHF membranes was quantified using AFM analysis. Figure 5a–d presents the AFM 3D images and average roughness values (Ra). The authors report that the surface roughness of the SPPSu/PPSu membrane, without the addition of TiO_2, was measured to be approximately 8 nm. However, upon incorporating different concentrations of TiO_2 nanoparticles into the SPPSu matrix in the inner surface, the roughness of the membranes increased significantly. Specifically, the roughness values were measured as 12 nm, 15 nm, and 21 nm for SPPSu-TiO_2 (0.50 wt%)/PPSu, SPPSu-TiO_2 (1.0 wt%)/PPSu, and SPPSu-TiO_2 (2.0 wt%)/PPSu, respectively. The observed increase in surface roughness can be attributed to the incorporation of hydrophilic groups into the SPPSu polymer matrix. These hydrophilic moieties promote the sudden demixing of the solvent and water during the phase inversion process. Consequently, a greater degree of phase separation occurs, resulting in the formation of a rougher surface in the inner layer of the DLHF membranes.

Preprints (www.preprints.org) | NOT PEER-REVIEWED | Posted: 20 June 2023 doi:10.20944/preprints202306.1410.v1

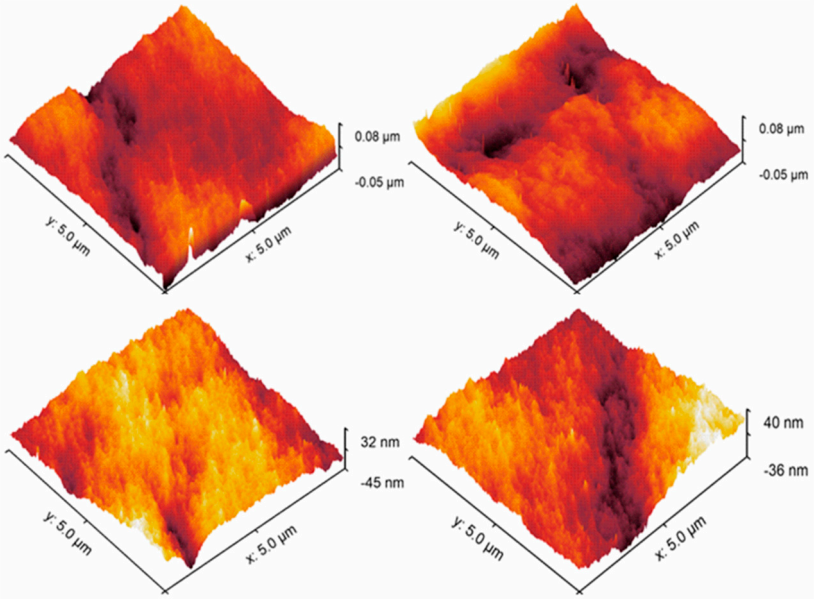

Figure 5. AFM 3D images of the DLHF membranes inner surface. (of (a) SPPSu/PPSu, (b) SPPSu-TiO_2 (0.50 wt%)/PPSu, (c) SPPSu-TiO_2 (1.0 wt%)/PPSu, and (d) SPPSu-TiO_2 (2.0 wt%)/PPSu.

3.3. Porosity and Hydrophilicity of membrane

The performance of membranes is greatly influenced by their surface properties, particularly porosity and hydrophilicity. In a study, these properties were investigated using overall porosity and contact angle measurements, and the results are presented in Figure 6. When examining the overall porosity, it was observed that the inclusion of TiO_2 nanoparticles in the SPPSu/PPSu DLHF nanocomposite membranes led to a significant increase in porosity compared to the pure SPPSu/PPSu membrane. The addition of TiO_2 resulted in an increase in the void volume within the substructure of the fibers, as evidenced by morphological studies. This suggests that the presence of TiO_2 nanoparticles contributes to the formation of a more porous membrane structure. The contact angle of the DLHF membrane, which indicates its hydrophilicity, exhibited a gradual decrease with increasing TiO_2 content in the SPPSu/PPSu DLHF inner surface. This can be attributed to the hydrophilic nature of TiO_2, which is attributed to the presence of hydroxyl groups on its surface. As the amount of TiO_2 increased, more hydroxyl groups were available to interact with the surrounding water molecules, leading to a decrease in the contact angle and an increase in hydrophilicity. However, it should be noted that the hydrophilicity of the membrane decreased when the TiO_2 content exceeded 1.0 wt%. This can be explained by the effects of agglomeration and irregular positioning of the TiO_2 particles within the membrane structure. These factors hindered the exposure of hydroxyl groups on the surface of the membrane, resulting in a reduction of hydrophilicity. In summary, the addition of TiO_2 nanoparticles to the SPPSu/PPSu nanocomposite DLHF membranes enhanced their overall porosity and hydrophilicity. The increased porosity can be attributed to the increased void volume within the fiber substructure. The improved hydrophilicity is a result of the hydroxyl groups present on the surface of TiO_2 nanoparticles, which interact with water molecules. However, excessive TiO_2 content can lead to agglomeration and irregular positioning, diminishing the availability of hydroxyl groups and subsequently reducing the membrane's hydrophilicity.

Preprints (www.preprints.org) | NOT PEER-REVIEWED | Posted: 20 June 2023 doi:10.20944/preprints202306.1410.v1

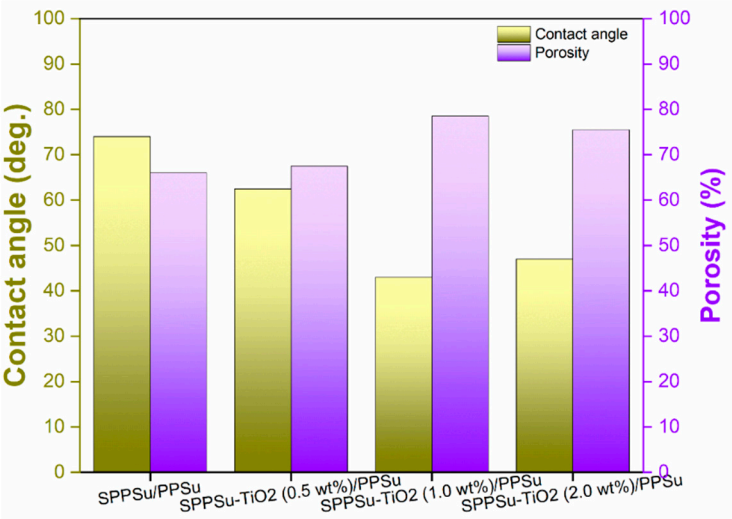

Figure 6. Water contact angle and porosity of the prepared DLHF membrane.

3.4. Zeta potential of membrane

Figure 7 provides valuable information on the zeta potential of the SPPSu/PPSu and SPPSu-TiO_2 (1.0 wt%)/PPSu nanocomposite DLHF membranes as a function of pH, ranging from 2.5 to 6. The zeta potential is a measure of the surface charge of a material and plays a significant role in various membrane processes, including fouling resistance. The results of the zeta potential measurements indicate that the addition of TiO_2 nanoparticles to the SPPSu polymer matrix in the inner layer of the DLHF membranes slightly increased the negative charge of the SPPSu-TiO_2 (1.0 wt%)/PPSu nanocomposite DLHF membranes compared to the SPPSu/PPSu DLHF membrane. At pH 6, the zeta potential of the SPPSu/PPSu membrane was measured to be -25 mV, while the SPPSu-TiO_2 (1.0 wt%)/PPSu nanocomposite DLHF membranes exhibited a zeta potential of -32 mV. This increase in negative charge can be attributed to the functional groups present in the TiO_2 nanoparticles. Furthermore, the incorporation of TiO_2 nanoparticles also resulted in a shift in the isoelectric point (IEP) of the membranes, which is the pH value at which there is virtually no charge present on the membrane surface. With the addition of TiO_2, the IEP of the DLHF membranes shifted to slightly higher pH values compared to the SPPSu/PPSu membrane. This indicates that the TiO_2 nanoparticles affected the membrane's surface charge characteristics. The negative potential observed in the DLHF membranes is beneficial for enhancing fouling resistance. The presence of a negative charge on the membrane surface leads to a charge repulsion mechanism, reducing the adhesion of foulants and improving the membrane's resistance to fouling. Therefore, the increase in negative zeta potential and the shift in IEP resulting from the incorporation of TiO_2 nanoparticles in the SPPSu-TiO_2 (1.0 wt%)/PPSu nanocomposite DLHF membranes suggest improved fouling resistance compared to the SPPSu/PPSu membrane. These findings highlight the importance of surface charge and zeta potential in membrane performance and provide valuable insights for the development and optimization of DLHF membranes with enhanced properties.

Preprints (www.preprints.org) | NOT PEER-REVIEWED | Posted: 20 June 2023 doi:10.20944/preprints202306.1410.v1

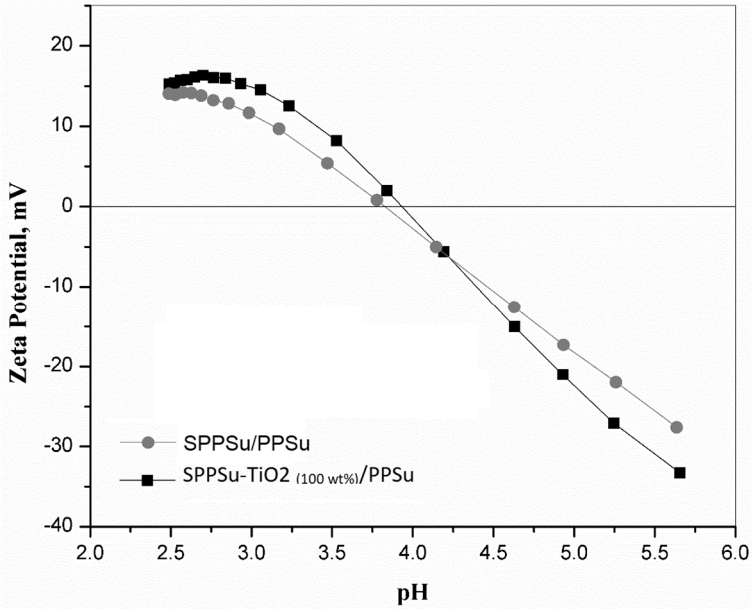

Figure 7. Membrane surface zeta potential with different pH.

3.5. Thermal stability of the membranes

The thermal stability of the prepared DLHF membrane was analyzed using Thermogravimetric analysis (TGA). TGA curves for both the SPPSu/PPSu membrane and the TiO_2-added SPPSu/PPSu nanocomposite membrane were obtained and are presented in Figure 8. These curves provide insights into the behavior of the membranes under different temperature conditions ranging from 100 to 600 °C. The incorporation of TiO_2 nanoparticles into the membrane led to an enhancement in its thermal resistance. The TGA curves of both the pristine and nanocomposite membranes exhibited three primary degradation steps. In the first degradation step, which occurred between 100 °C and 200 °C, a weight loss was observed. This initial weight loss was attributed to the volatilization of volatile components or the evaporation of residual absorbed water. It indicates the removal of any moisture or volatile matter present in the membranes. The second stage of degradation occurred between 200 °C and 550 °C. In this range, a higher weight loss was observed compared to the first stage. This weight loss was primarily attributed to the degradation of the polymeric chain in the membranes. As the temperature increased, the polymeric chains started to break down, resulting in a significant weight loss. Beyond 550 °C, the polymeric chains were completely broken, and the formation of ash began. This stage represents the carbonization of the degraded products, leading to the formation of ash residues. From the TGA analysis, it was concluded that the nanocomposite membrane with TiO_2 nanoparticles exhibited higher thermal stability compared to the pristine SPPSu/PPSu membrane. The incorporation of TiO_2 nanoparticles into the DLHF structure enhanced the thermal resistance of the nanocomposite membrane, as evidenced by its ability to withstand higher temperatures without significant weight loss or degradation. Overall, the TGA study provided valuable information about the thermal stability of the prepared DLHF membranes. The presence of TiO_2 nanoparticles improved the membrane's resistance to thermal degradation, indicating its potential for applications where high-temperature stability is required.

Preprints (www.preprints.org) | NOT PEER-REVIEWED | Posted: 20 June 2023 doi:10.20944/preprints202306.1410.v1

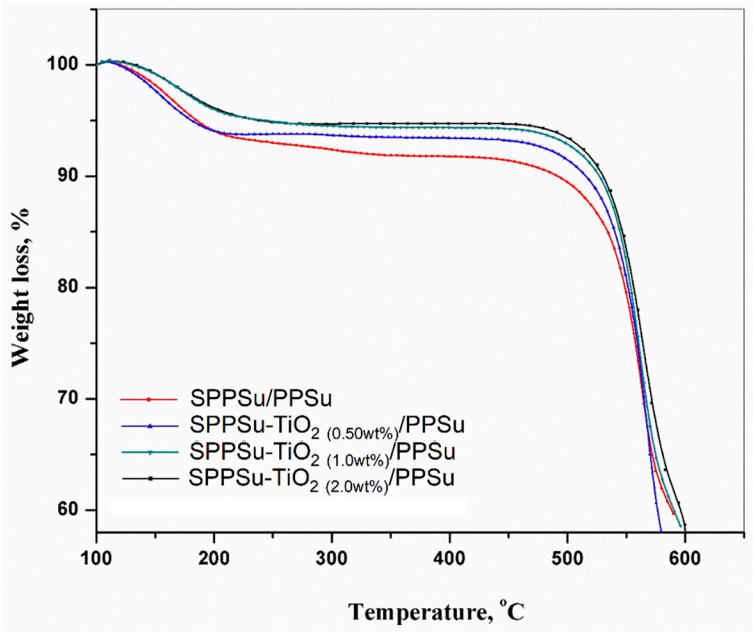

Figure 8. Thermogravimetric analysis of the prepared DLHF membrane.

3.6. Mechanical properties of the membranes

The mechanical properties of the prepared DLHF membrane were investigated and depicted in Figure 9. The relationship between tensile stress and tensile strain was examined to evaluate the membrane's performance under mechanical load. A high tensile modulus indicates that the membrane possesses high rigidity. This means that it can resist deformation and maintain its shape under applied stress. The combination of high tensile stress and strain at break is an important characteristic of toughness in materials. It suggests that the membrane can endure significant stretching before reaching its breaking point, indicating enhanced durability. The introduction of TiO_2 nanoparticles into the DLHF membrane played a crucial role in modifying its mechanical properties. The presence of these nanoparticles resulted in an improvement in the stress values at break. In other words, the membrane became stronger and more resistant to fracture due to the inclusion of TiO2 nanoparticles in the fiber membranes. By adding 0.5 to 2wt% of nanoparticles in the inner layer of the nanocomposite hollow fiber, the tensile stress increased, while the strain decreased. This indicates that the addition of nanoparticles to the SPPSu/PPSu composite material enhances the tensile strength of the membranes. The stress values of the membranes are as follows: SPPSu/PPSu (2.4 MPa), SPPSu-TiO_2 (0.5 wt%)/PPSu (3.1 MPa), SPPSu-TiO_2 (1.0 wt%)/PPSu (3.4 MPa), and SPPSu-TiO_2 (2.0 wt%)/PPSu (3.9 MPa). These values indicate that the addition of TiO_2 nanoparticles led to a significant increase in the tensile stress compared to the pristine SPPSu/PPSu membrane. It is important to note that the concentration of nanoparticles influenced the mechanical properties. Specifically, the addition of 0.5 to 1.0 wt% of TiO_2 nanoparticles resulted in improved mechanical properties, while the addition of 2.0 wt% did not yield further improvements. This suggests that an optimal concentration of 1.0 wt% was sufficient to enhance the mechanical performance of the nanocomposite membrane. In conclusion, the incorporation of TiO2 nanoparticles into the DLHF membrane structure resulted in improved mechanical properties. The nanocomposite membranes exhibited higher tensile stress and increased toughness compared to the pristine membrane. These findings highlight the potential of using TiO_2 nanoparticles as a means to enhance the mechanical performance of composite membranes.

Preprints (www.preprints.org) | NOT PEER-REVIEWED | Posted: 20 June 2023 doi:10.20944/preprints202306.1410.v1

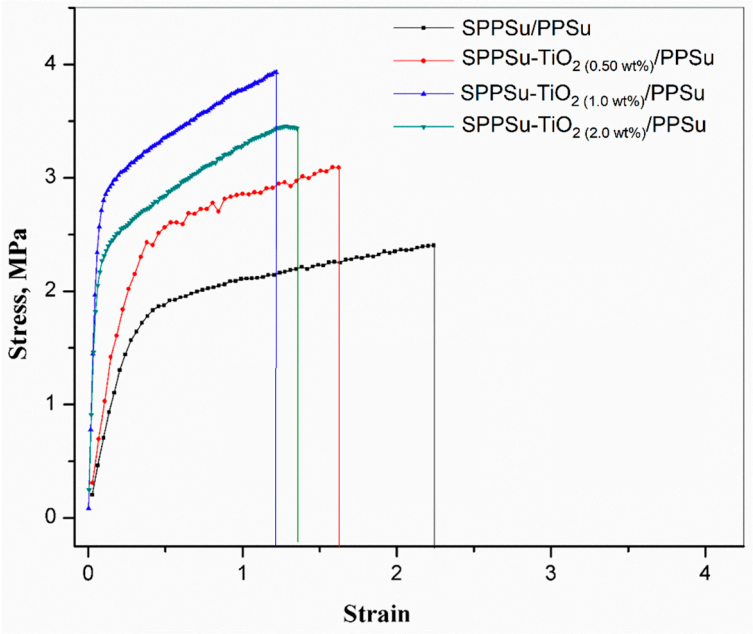

Figure 9. Mechanical properties of the prepared DLHF membranes.

3.7. Performance of membrane

The experimental evaluation of membrane performance in water permeation using a cross-flow set-up revealed significant improvements in the pure water fluxes of DLHF nanocomposite membranes compared to the pure membrane. The water permeability values for the different DLHF membranes were obtained as follows: SPPSu/PPSu (2.5 L/m²h.bar), SPPSu-TiO_2 (0.50 wt%)/PPSu (3.5 L/m²h.bar), SPPSu-TiO_2 (1.0 wt%)/PPSu (5.1 L/m²h.bar), and SPPSu-TiO_2 (2.0 wt%)/PPSu (5.4 L/m²h.bar). These results, presented in Figure 10, clearly demonstrated that the incorporation of TiO_2 nanoparticles into the inner-layer of the SPPSu polymer matrix led to a substantial enhancement in water permeability. The observed increase in water permeability can be attributed to multiple factors. Firstly, the addition of TiO_2 nanoparticles influenced the pure water flux, resulting in improved water permeability. TiO_2 nanoparticles have a high affinity for water molecules, leading to increased hydrophilicity of the membrane surface. The enhanced hydrophilicity facilitated the passage of water molecules through the membrane, thereby boosting water permeability. Furthermore, the effects of TiO_2 nanoparticle incorporation on the membrane morphology played a crucial role in determining the permeation properties. The addition of nanoparticles altered the membrane structure and resulted in changes in pore size, porosity, and surface roughness. These modifications could create more favorable conditions for water transport, contributing to the increased water permeability observed in the nanocomposite membranes. The findings of this study shed light on the design and optimization of DLHF membranes for efficient water permeation applications. Future research can explore the potential of other nanomaterials as additives to further enhance membrane performance.

Preprints (www.preprints.org) | NOT PEER-REVIEWED | Posted: 20 June 2023 doi:10.20944/preprints202306.1410.v1

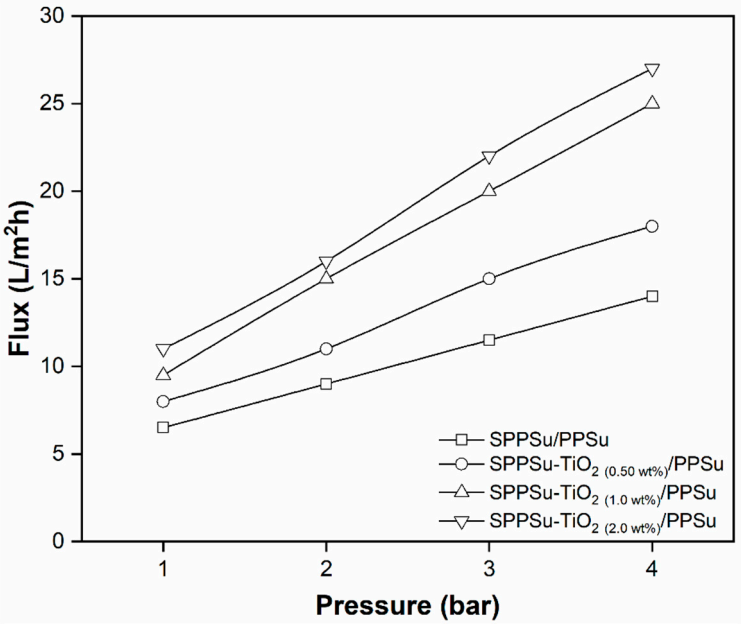

Figure 10. Water permeability of prepared DLHF membranes.

The rejection performance of prepared pure SPPSu/PPSu and SPPSu-TiO_2/PPSu nanocomposite DLHF membranes was evaluated using Na_2SO_4 and Mg_2SO_4 as model salts. A simulated salt solution with a concentration of 500 ppm and a neutral pH was employed as the feed solution. The rejection results are depicted in Figures 11 and 12. The incorporation of TiO_2 in the inner layer of SPPSu/PPSu nanocomposite DLHF membranes exhibited higher rejection compared to the pure SPPSu/PPSu DLHF membranes. The rejection percentages for Mg_2SO_4 and Na_2SO_4 salts for the different membrane compositions are as follows: SPPSu/PPSu: Mg_2SO_4 rejection-56%, Na_2SO_4 rejection -45%, SPPSu-TiO_2 (0.50 wt%)/PPSu: Mg_2SO_4 rejection-81%, Na_2SO_4 rejection-78%, SPPSu-TiO_2 (1.0 wt%)/PPSu: Mg_2SO_4 rejection-94%, Na_2SO_4 rejection -86%, and SPPSu-TiO_2 (2.0 wt%)/PPSu: Mg_2SO_4 rejection -95%, Na_2SO_4 rejection -91%, respectively. The results clearly indicate that the incorporation of TiO_2 nanoparticles in the inner layer of SPPSu/PPSu nanocomposite DLHF membranes significantly enhances the rejection performance for both Mg_2SO_4 and Na_2SO_4 salts. The rejection percentages show a noticeable increase with an increase in TiO_2 content. This enhancement can be attributed to several factors, including the unique properties of TiO_2 nanoparticles and the modified membrane structure.

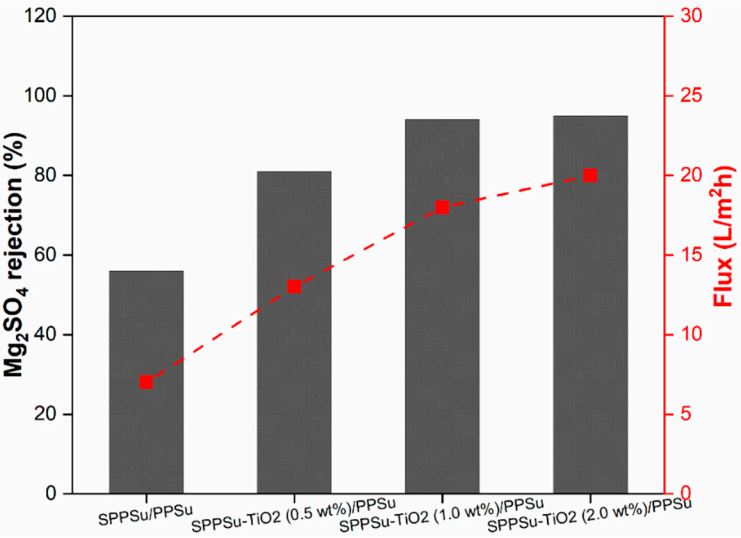

Figure 11. Mg_2SO_4 rejection and flux performance of prepared DLHF membranes.

Preprints (www.preprints.org) | NOT PEER-REVIEWED | Posted: 20 June 2023 doi:10.20944/preprints202306.1410.v1

The rejection mechanism of the nanocomposite DLHF membranes can be explained by several phenomena. Firstly, the presence of TiO_2 nanoparticles in the inner layer introduces additional tortuous pathways for solute transport, resulting in increased diffusion path lengths and improved rejection. This can be attributed to the increased surface area of the membranes and the resulting longer diffusion paths, which hinder the passage of salt ions. Secondly, the TiO_2 nanoparticles may contribute to the formation of a more compact and dense membrane structure, leading to reduced pore size and increased selectivity. The enhanced rejection can also be attributed to the electrostatic interactions between the TiO_2 nanoparticles and the salt ions, as TiO_2 is known to possess surface charges that can facilitate the rejection of charged species. Furthermore, the nanocomposite DLHF membranes demonstrated comparable permeation flux to that of pure water flux, indicating minimal flux decline due to the incorporation of TiO_2 nanoparticles. This suggests that the presence of TiO_2 in the nanocomposite membranes does not significantly impede water permeation, indicating their potential for practical applications in water treatment processes. Overall, the incorporation of TiO_2 nanoparticles in the inner layer of SPPSu/PPSu nanocomposite DLHF membranes leads to improved rejection performance for both Na_2SO_4 and Mg_2SO_4 salts. The rejection mechanism involves increased diffusion path lengths, modified membrane structure, and potential electrostatic interactions. The nanocomposite membranes exhibit high rejection while maintaining permeation flux comparable to pure water, highlighting their potential for water treatment applications. Further research can focus on optimizing the TiO_2 nanoparticle content and exploring the long-term stability and durability of the nanocomposite DLHF membranes.

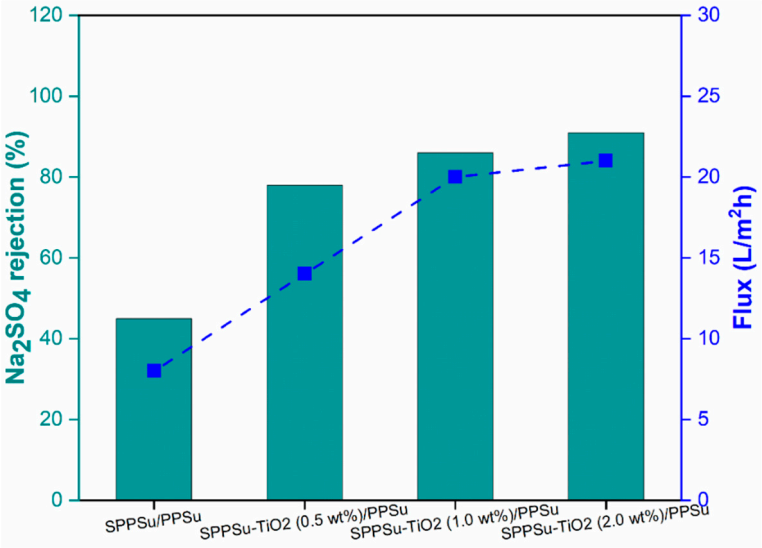

Figure 12. Na_2SO_4 rejection and flux performance of prepared DLHF membranes.

4. Conclusions

This study investigated the effects of incorporating TiO_2 nanoparticles into SPPSu/PPSu DLHF. The SEM images of the cross section morphology revealed a moderately symmetric structure in both the inner and outer layers of the membranes, despite the observed delamination between the layers. The addition of TiO_2 nanoparticles resulted in significant structural changes, including the formation of a thin top layer with nanopores and microvoids in the outer layer. The surface roughness of the inner layer increased with the incorporation of TiO_2 nanoparticles, indicating a rougher surface. The inclusion of TiO_2 nanoparticles led to increased overall porosity and hydrophilicity of the DLHF membranes. The addition of TiO_2 resulted in a more porous membrane structure and a decrease in the contact angle, indicating improved water permeability and enhanced hydrophilicity. However, excessive TiO_2 content (>1.0 wt%) led to agglomeration and irregular positioning of the nanoparticles, reducing the membrane's hydrophilicity. The zeta potential measurements showed that the incorporation of TiO_2 nanoparticles slightly increased the negative charge of the nanocomposite DLHF membranes compared to the pure membrane. This increase in negative zeta potential and the

shift in isoelectric point suggest improved fouling resistance for the nanocomposite membranes. The thermal stability of the nanocomposite membranes was enhanced with the incorporation of TiO_2 nanoparticles, as indicated by the TGA analysis. The nanocomposite membranes exhibited higher tensile stress and increased toughness compared to the pure membrane, demonstrating improved mechanical properties. In terms of performance, the nanocomposite DLHF membranes showed significant improvements in pure water flux compared to the pure membrane. The water permeability increased with the addition of TiO_2 nanoparticles, attributed to their hydrophilic nature and the modifications in membrane morphology. The rejection performance of the nanocomposite membranes was evaluated using Na_2SO_4 and Mg_2SO_4 as model salts. The incorporation of TiO_2 nanoparticles in the inner layer of the nanocomposite membranes resulted in higher rejection percentages for both salts compared to the pure membrane. The rejection increased with increasing TiO_2 content, indicating improved salt rejection performance.

Overall, the incorporation of TiO_2 nanoparticles into SPPSu/PPSu DLHF membranes enhanced their structural, surface, thermal, mechanical, water permeability, and rejection properties. These findings provide valuable insights for the development and optimization of DLHF membranes with enhanced performance for various applications, including water treatment and desalination.

Author Contributions: Conceptualization, J.A. and A.K.S.; methodology, J.A.; software, A.K.S.; validation, J.A. and A.K.S.; formal analysis, L.A.; investigation, A.K.S, and J.A.; resources, M.A.; data curation, J.A.; writing—original draft preparation, J.A. and A.K.S; writing—review and editing, J.A. and A.K.S; visualization, J.A. and M.A.; supervision, M.A.; project administration, J.A.; funding acquisition, J.A. and L.A. All authors have read and agreed to the published version of the manuscript.

Funding: This work was funded by the National Plan for Science, Technology and Innovation (MAARIFAH), King Abdulaziz City for Science and Technology, Kingdom of Saudi Arabia, Award Number 12-ADV2611-02.

Institutional Review Board Statement: Not applicable

Data Availability Statement: Not applicable

Acknowledgments: This work was funded by the National Plan for Science, Technology and Innovation (MAARIFAH), King Abdulaziz City for Science and Technology, Kingdom of Saudi Arabia, Award Number 12-ADV2611-02.

Conflicts of Interest: The authors declare no conflict of interest.

References

1. Anis, S.F.; Hashaikeh, R.; Hilal, N. Reverse osmosis pretreatment technologies and future trends: A comprehensive review. *Desalination* **2019**, *452*, 159–195.
2. Tong, T.; Elimelech, M. The Global Rise of Zero Liquid Discharge for Wastewater Management: Drivers, Technologies, and Future Directions. *Environ. Sci. Technol.* **2016**, *50*, 6846–6855.
3. Li, C.; Li, S.; Zhang, J.; Yang, C.; Su, B.; Han, L.; Gao, X. Emerging sandwich-like reverse osmosis membrane with interfacial assembled covalent organic frameworks interlayer for highly-efficient desalination. *J. Memb. Sci.* **2020**, *604*, 118065.
4. Lin, Y.; Chen, Y.; Wang, R. Thin film nanocomposite hollow fiber membranes incorporated with surface functionalized HKUST-1 for highly-efficient reverses osmosis desalination process. *J. Memb. Sci.* **2019**, *589*, 117249.
5. Noraaini, A.; Sofiah, H.; Asmadi, A.; Suriyani, A.R. Fabrication and characterization of asymmetric ultrafiltration membrane for BSA separation: Effect of sheer rates. *J. Appl. Sci.* **2010**, *10*, 1083–1089.
6. Eykens, L.; De Sitter, K.; Dotremont, C.; Pinoy, L.; Van Der Bruggen, B. How to Optimize the Membrane Properties for Membrane Distillation: A Review. *Ind. Eng. Chem. Res.* **2016**, *55*, 9333–9343.
7. Wang, M.; Wu, L.G.; Mo, J.X.; Gao, C.J. The preparation and characterization of novel charged polyacrylonitrile/ PES-C blend membranes used for ultrafiltration. *J. Memb. Sci.* **2006**, *274*, 200–208.
8. Karanasiou, A.; Kostoglou, M.; Karabelas, A. An experimental and theoretical study on separations by vacuum membrane distillation employing hollow-fiber modules. *Water (Switzerland)* **2018**, *10*.
9. Parashuram, K.; Maurya, S.K.; Rana, H.H.; Singh, P.S.; Ray, P.; Reddy, A.V.R. Tailoring the molecular weight cut off values of polyacrylonitrile based hollow fibre ultrafiltration membranes with improved fouling resistance by chemical modification. *J. Memb. Sci.* **2013**, *425–426*, 251–261.

10. Liu, T.-Y.; Tong, Y.; Liu, Z.-H.; Lin, H.-H.; Lin, Y.-K.; Van der Bruggen, B.; Wang, X.-L. Extracellular polymeric substances removal of dual-layer (PES/PVDF) hollow fiber UF membrane comprising multi-walled carbon nanotubes for preventing RO biofouling. *Sep. Purif. Technol.* **2015**, *148*, 57–67.
11. Bóna, Á.; Varga, Á.; Galambos, I.; Nemestóthy, N. Dealcoholization of Unfiltered and Filtered Lager Beer by Hollow Fiber Polyelectrolyte Multilayer Nanofiltration Membranes—The Effect of Ion Rejection. *Membranes (Basel).* **2023**, *13*, 283.
12. Jasim, D.J.; Mohammed, T.J.; Harharah, H.N.; Harharah, R.H.; Amari, A.; Abid, M.F. Modeling and Optimal Operating Conditions of Hollow Fiber Membrane for CO 2 / CH 4 Separation. *Membranes (Basel).* **2023**, *13*, 557.
13. Bet-moushoul, E.; Mansourpanah, Y.; Farhadi, K.; Tabatabaei, M. TiO2 nanocomposite based polymeric membranes: a review on performance improvement for various applications in chemical engineering processes. *Chem. Eng. J.* **2015**, *283*, 29–46.
14. Zhu, W.P.; Sun, S.P.; Gao, J.; Fu, F.J.; Chung, T.S. Dual-layer polybenzimidazole/polyethersulfone (PBI/PES) nanofiltration (NF) hollow fiber membranes for heavy metals removal from wastewater. *J. Memb. Sci.* **2014**, *456*, 117–127.
15. Liu, Y.; Liu, T.; Su, Y.; Yuan, H.; Hayakawa, T.; Wang, X. Fabrication of a novel PS4VP/PVDF dual-layer hollow fiber ultrafiltration membrane. *J. Memb. Sci.* **2016**, *506*, 1–10.
16. Liu, T.Y.; Zhang, R.X.; Li, Q.; Van der Bruggen, B.; Wang, X.L. Fabrication of a novel dual-layer (PES/PVDF) hollow fiber ultrafiltration membrane for wastewater treatment. *J. Memb. Sci.* **2014**, *472*, 119–132.
17. Liu, T.Y.; Li, C.K.; Pang, B.; Van der Bruggen, B.; Wang, X.L. Fabrication of a dual-layer (CA/PVDF) hollow fiber membrane for RO concentrate treatment. *Desalination* **2015**, *365*, 57–69.
18. Chung, T.S.N. Fabrication of Hollow-Fiber Membranes by Phase Inversion. *Adv. Membr. Technol. Appl.* **2008**, 821–839.
19. Dzinun, H.; Othman, M.H.D.; Ismail, A.F.; Puteh, M.H.; Rahman, M.A.; Jaafar, J. Morphological study of co-extruded dual-layer hollow fiber membranes incorporated with different TiO2 loadings. *J. Memb. Sci.* **2015**, *479*, 123–131.
20. Shukla, A.K.; Alam, J.; Alhoshan, M. Recent Advancements in Polyphenylsulfone Membrane Modification Methods for Separation Applications. *Membranes (Basel).* **2022**, *12*, 1–35.
21. Bassyouni, M.; Abdel-Aziz, M.H.; Zoromba, M.S.; Abdel-Hamid, S.M.S.; Drioli, E. A review of polymeric nanocomposite membranes for water purification. *J. Ind. Eng. Chem.* **2019**, *73*, 19–46.
22. Singh, S.; Varghese, A.M.; Reddy, K.S.K.; Romanos, G.E.; Karanikolos, G.N. Polysulfone Mixed-Matrix Membranes Comprising Poly(ethylene glycol)-Grafted Carbon Nanotubes: Mechanical Properties and CO2Separation Performance. *Ind. Eng. Chem. Res.* **2021**, *60*, 11289–11308.
23. Sinha, M.K.; Purkait, M.K. Increase in hydrophilicity of polysulfone membrane using polyethylene glycol methyl ether. *J. Memb. Sci.* **2013**, *437*, 7–16.
24. Eke, J.; Mills, P.A.; Page, J.R.; Wright, G.P.; Tsyusko, O. V.; Escobar, I.C. Nanohybrid membrane synthesis with phosphorene nanoparticles: A study of the addition, stability and toxicity. *Polymers (Basel).* **2020**, *12*.
25. Hamid, N. a a; Ismail, a. F.; Matsuura, T.; Zularisam, a. W.; Lau, W.J.; Yuliwati, E.; Abdullah, M.S. Morphological and separation performance study of polysulfone/titanium dioxide (PSF/TiO2) ultrafiltration membranes for humic acid removal. *Desalination* **2011**, *273*, 85–92.
26. Khalid, A.; Ibrahim, A.; Al-Hamouz, O.C.S.; Laoui, T.; Benamor, A.; Atieh, M.A. Fabrication of polysulfone nanocomposite membranes with silver-doped carbon nanotubes and their antifouling performance. *J. Appl. Polym. Sci.* **2017**, *134*, 1–12.
27. Karkooti, A.; Yazdi, A.Z.; Chen, P.; McGregor, M.; Nazemifard, N.; Sadrzadeh, M. Development of advanced nanocomposite membranes using graphene nanoribbons and nanosheets for water treatment. *J. Memb. Sci.* **2018**, *560*, 97–107.
28. Ihsanullah; Laoui, T.; Al-Amer, A.M.; Khalil, A.B.; Abbas, A.; Khraisheh, M.; Atieh, M.A. Novel anti-microbial membrane for desalination pretreatment: A silver nanoparticle-doped carbon nanotube membrane. *Desalination* **2015**, *376*, 82–93.
29. Shukla, A.K.; Alam, J.; Ali, F.A.A.; Alhoshan, M. Efficient soluble anionic dye removal and antimicrobial properties of ZnO embedded- polyphenylsulfone membrane. *Water Environ. J.* **2021**, *35*, 670–684.
30. Hairom, N.H.H.; Mohammad, A.W.; Kadhum, A.A.H. Influence of zinc oxide nanoparticles in the nanofiltration of hazardous Congo red dyes. *Chem. Eng. J.* **2015**, *260*, 907–915.
31. Potts, J.R.; Dreyer, D.R.; Bielawski, C.W.; Ruoff, R.S. Graphene-based polymer nanocomposites. *Polymer (Guildf).* **2011**, *52*, 5–25.